THz Near-field spectroscopy of metamaterial resonators

THz Near-field spectroscopy of metamaterial resonators

R Degl'Innocenti,[1] Y Lu,[2] L L Hale,[3] A M Zaman,[2] S J Addamane,[4] I Brener,[4] O Mitrofanov[3]

[1]School of Electronic Engineering and Computer Science, Queen Mary University of London
[2]School of Engineering, Lancaster University, United Kingdom
[3]Electronic and Electrical Engineering, University College London, United Kingdom
[4]Center for Integrated Nanotechnologies, Sandia National Laboratories, United States

r.deglinnocenti@qmul.ac.uk

Abstract. Terahertz near-field spectroscopy is a powerful technique for the investigation of metamaterial resonators with subwavelength resolution. Here, we used an a-SNOM THz time domain spectroscopic system for the direct study of all the modes supported by individual D-split ring resonators, their E-field distributions and relative Q factors. A cross-polarized excitation and detection technique is also demonstrated, yielding a modes' mapping by the resonators with unprecedented resolution and sharpness.

1. Introduction

Metamaterials provide an efficient and versatile platform for the realization of integrated terahertz (THz) devices, ranging from modulators [1-3] to detectors [4, 5], sources [6] and sensing elements [7]. Metamaterials consist of subwavelength artificial atoms which can support several modes. The investigation of these modes' nature and properties, e.g. their coupling to free space (bright or dark modes), their E-field distributions and relative Q-factors is crucial for the tailoring of their specific functionalities and for the design of more efficient devices. Typically, the characterization of these objects is performed by using standard far-field techniques, e.g. THz time domain spectroscopy, which rely on large arrays composed of identical metamaterial units, to ease light coupling. However, this analysis is based on indirect measurements, since they are modified by the coupling between neighbouring metamaterial units [8], and it is often less effective in detection of low-radiative, dark modes. THz near-field imaging techniques [8-13], instead, allow the investigation of individual metamaterial units, the direct retrieval of single resonator's Q-factor, and the acquisition of the E-field distribution of the excited modes. Further to this, near-field spectroscopy does not require the fabrication of large arrays to investigate a single metamaterial design. In this study, a THz broadband a-SNOM was used to address individual metallic asymmetric D-split-ring THz resonators (ADSRs) [14].

2. Results

All the samples used were realised via optical lithography (Ti/Au (10/150 nm) metallic thermal evaporation and lift off on a Silicon substrate. A THz near-field probe with a subwavelength size aperture and an integrated THz detector was placed at closed proximity to the sample's surface (~5 μm) to directly probe the evanescent electric field components of all the modes supported by the metamaterial resonator [8]. Raster-scan THz a-SNOM imaging was combined with the THz time-domain

spectroscopy analysis, which allowed simultaneous excitation of all of the modes and their selective detection with a subwavelength spatial resolution of a few μm.

A preliminary mode mapping on an array (array 1) composed of identical metamaterial units was performed in far-field by using a commercial THz-TDS system from MenloSystems, model K15. An optical picture of array 1 together with the main lithographic parameters, reported in Table 1, is shown

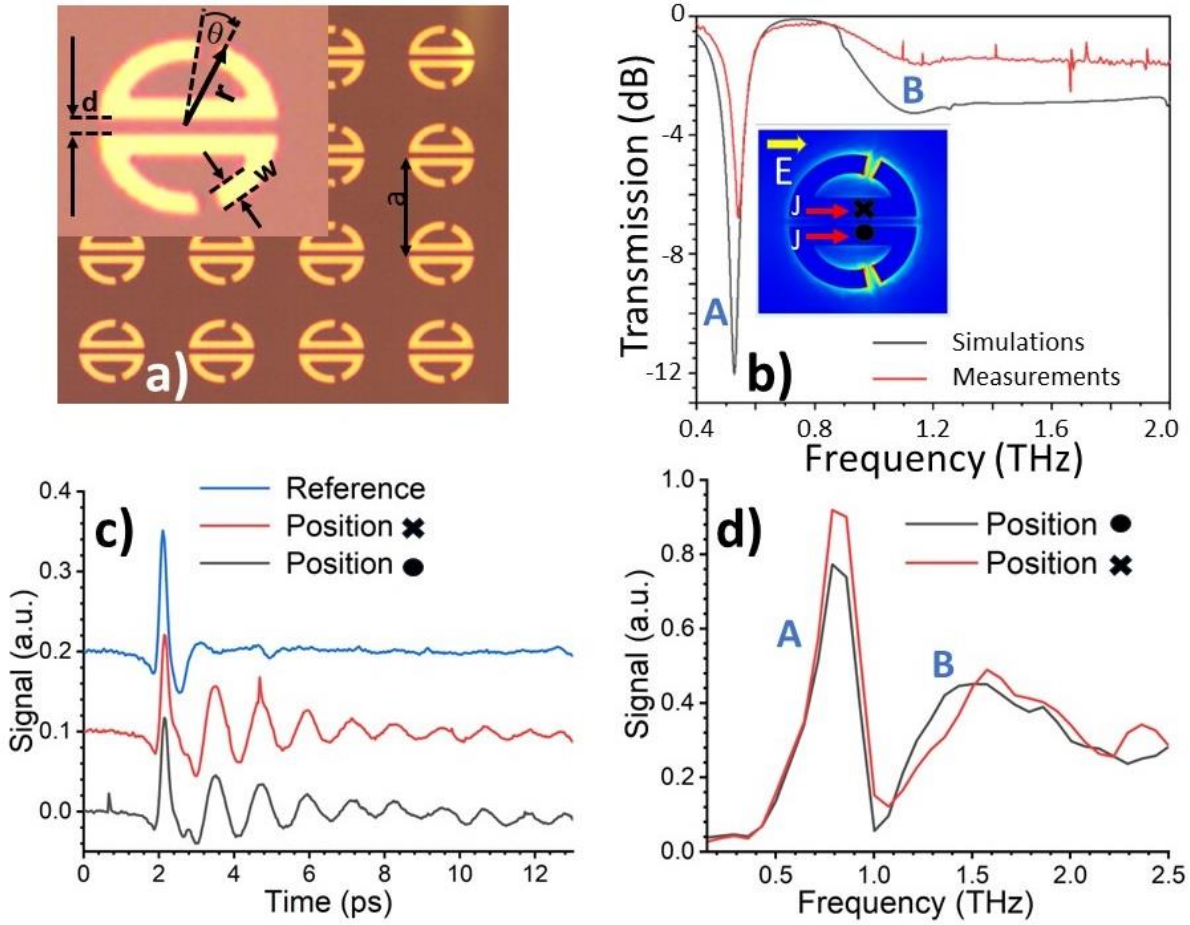

Figure 1: a) Optical image of the ADSR MM array resonator, inset: a unit cell illustrating the resonator's parameters, reported in Table 1. b) Simulated and measured far field transmission spectra for the uniform ADSR array showing the first two supported modes **A** and **B**. Inset: Simulated spatial profiles of mode **A** (normalized E-field at 2 μm height from the surface) together with a sketch of the induced surface currents **J** and marks for the two positions where the near-field time-domain waveforms were measured. c) Near-field THz pulse waveforms measured at the two locations marked in (b). d) Fourier transformed signals normalized to the reference of the time waveforms shown in c); Modes **A** and **B** are clearly identified.

in Figure 1 a). When the incident E-field of the incoming THz pulses is oriented along the direction of the ADSRs' bars, as showed in the inset of Figure 1 b), two main modes, A and B, centred respectively at 0.54 THz and 1.15 THz are excited. The experimental measurements are in very good agreement with the simulations performed with finite element method software Comsol Multiphysics also showed in Figure 1 b).

A second array (array 2) was then specifically fabricated for the near field measurements. In this array, a lithographic tuning on each single resonator was performed, and the designs were optimized to exhibit the main resonance at the maximum sensitivity of the near field probe, approximately ~0.8 THz. We focused on three different resonators in array 2, whose design's parameters are also reported in Table 1. Figure 1 c) presents the time domain waveforms acquired when the probe was positioned on the ADSR central bars, as showed in the inset of Figure 1 b) and out of the resonators' area for resonator #1. In

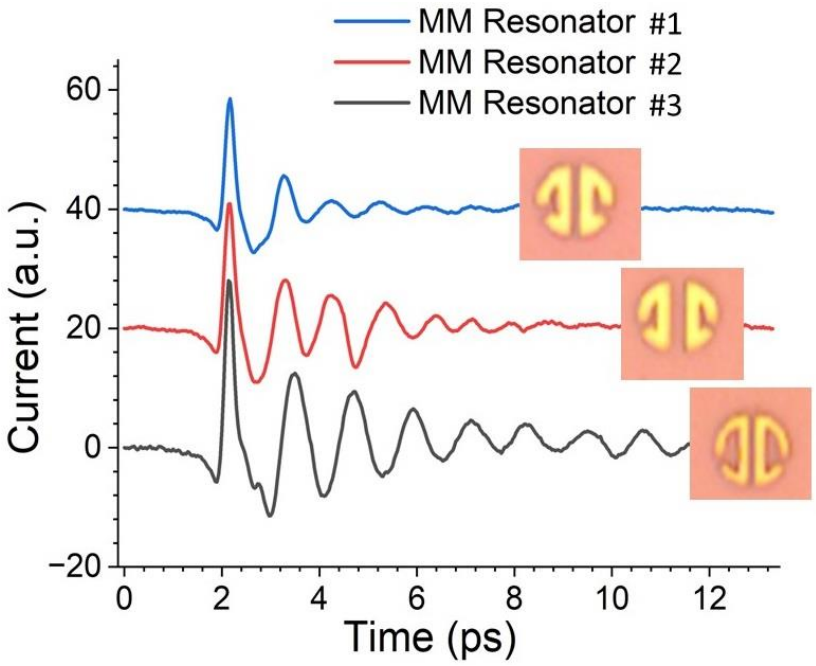

Figure 2; Resonant time waveforms for the three different ADSRs acquired at the maximum signal.

correspondence of the central bars, where the surface currents **J** are excited, a clear ringing is observed. The normalized fast Fourier Transform signal of these waveforms is reported in Figure 1 d) showing again mode A and B, consistently with the measurements and simulations performed in far-field for

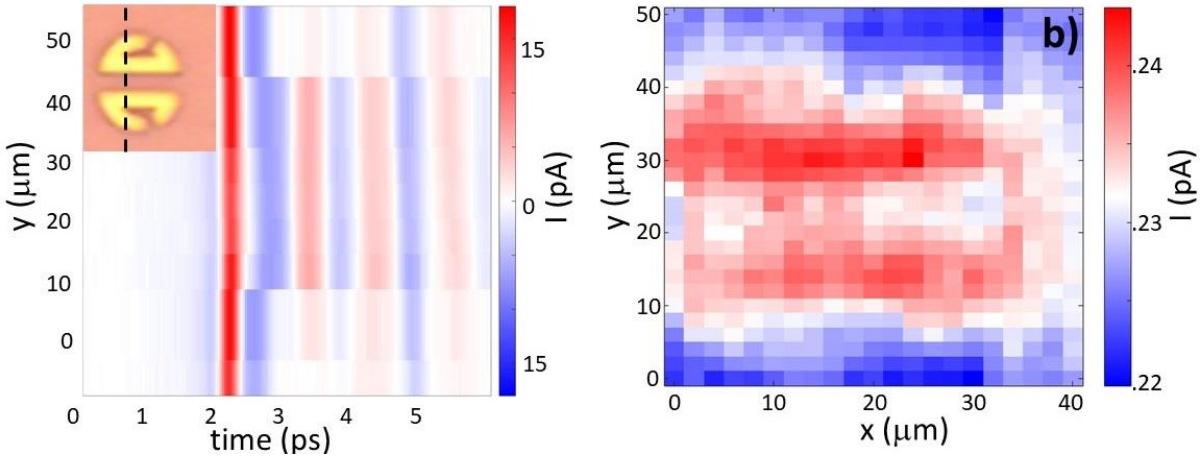

Figure 2; a)) Space−time scan across ADSR #2. The signal oscillation is maximal in the resonator center. b) Spatial map taken across the same resonator at a time corresponding to a peak in resonant time-domain waveform.

array 1. The three resonators have different Q factors, as can be noticed by the different ringing in Figure 2. All the time waveforms have been acquired on the bottom central bar, at the same position as in the inset of Fig. 1 b). The temporal evolution of the excited modes allows us to directly calculate the Q-factors of the resonators by using the single harmonic oscillation model [9]. The time domain waveform y(t) can be described as:

$$y(t) = \alpha e^{-\gamma t} cos(\omega t - \varphi) \quad (1)$$

Where α is the amplitude, γ is the decay rate, ω is the resonant frequency of the main oscillation. The Q-factor of the oscillation is then given by:

$$Q = \frac{\omega}{2\gamma} \tag{2}$$

Table 1. Parameters of the ADSRs investigated

ADSR	r (μm)	d (μm)	**a** (μm)	θ (deg)	w (μm)	β (deg)	Q factor
Array 1	30.3	3.4	100	15	8.4	14	12±1
Array 2- #1	20.2	3.4	600	20	6	15	11±1
Array 2- #2	20.2	9	600	20	8.4	15	7±1
Array 2- #3	20.2	3.4	600	20	8.4	20	3±1

The Q factors for the 3 resonators are reported in Table 1 together with the Q factor calculated for array 1 from the THz-TDS measurements. A space-time scan across resonator #2, presented in Figure 3, showed a maximum ringing in the central part of the ADSR, fast decaying elsewhere. A spatial map, performed by fixing the time delay to a maximum peak of the time waveform and moving the sample in the xy plane at a fixed distance z with the probe, is presented in Figure 2 b), confirming that the maximum E-field signal is recorded on top of the central bars of the metamaterial, suggesting that the maximal signal is related to the surface currents **J** excited in the resonators [11]. A further set of measurements were acquired in cross-polarized configuration, with orthogonal excitation and detection. The probe and sample are kept at the same relative position, whilst the incoming THz polarisation is rotated by 90° as showed in Figure 4 a). The probe will then be able to detect the orthogonal components

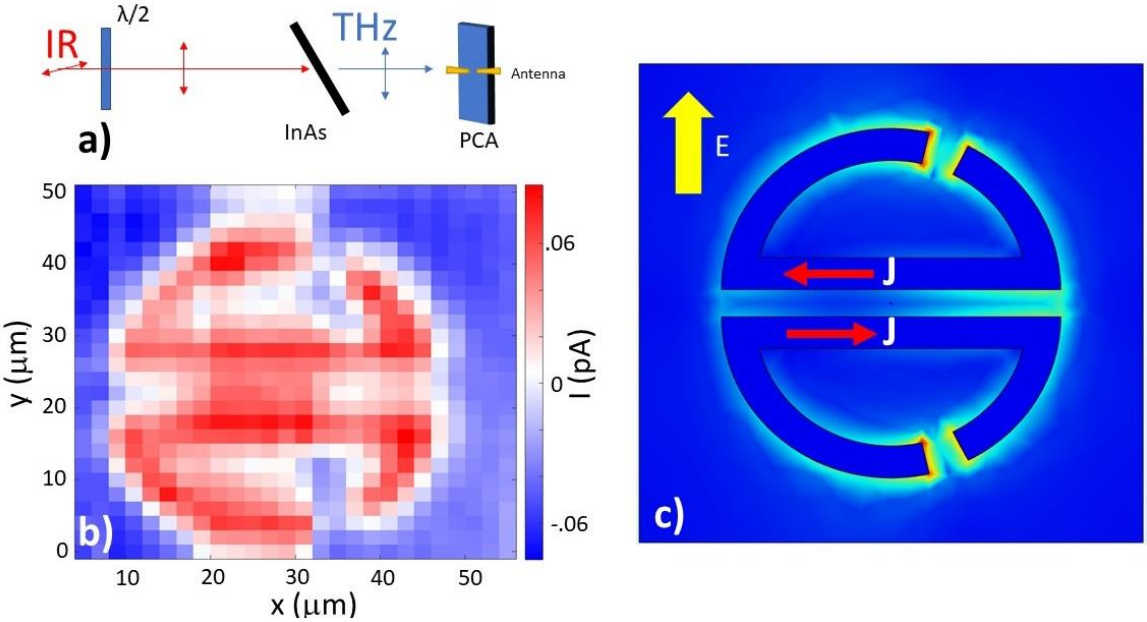

Figure 4: a) Cross-polarized excitation and detection scheme and b) spatial map taken across ADSR #1 at a peak of the time waveform. c) Simulated spatial profiles of the first mode (normalized E-field at 2 μm height from the surface) excited in this configuration.

of the modes' E-field supported by the resonator. In this configuration, the incoming E-field excites several modes, bright and dark ones, at the same time with different relative weights [9]. An unprecedented contrast and spatial resolution, beyond the 10 μm probe size, can be observed in the map acquired for resonator #1 at a fixed time delay and presented in Figure 4 b). The simulated mode profile of the lowest frequency supported mode is showed in Figure 4 c) for completeness.

In conclusion, THz-TDS near-field spectroscopy allows the investigation of all the modes supported by individual ADSR resonators, the retrieval of the Q-factors and of E-field distributions. The near-field

imaging technique provides a unique tool for several research areas ranging from the development of novel THz optoelectronic platforms [15, 16], e.g. efficient sources and active devices, to fundamental investigation in photonics, such as bound-in-continuum states [17], to the realization of high-Q resonators, e.g. for higher spectral resolution THz sensors.

Acknowledgments
SNL is managed and operated by NTESS under DOE NNSA contract DE-NA0003525. This work was supported by the US Department of Energy (DOE), Office of Basic Energy Sciences, Division of Materials Sciences and Engineering and performed, in part, at the Center for Integrated Nanotechnologies, an Office of Science User Facility operated for the US DOE Office of Science.

References

[1] Degl'Innocenti R, Lin H, Navarro-Cia M 2022 *Nanophoton.* **11**(8) 1485-1514.
[2] Zaman A M et al 2022 *IEEE Trans. Terahertz Scie.* **12**(5) 520-6.
[3] Zaman A M et al 2023 *Front. Nanotechnol. Sec. Nanophotonics* **5** DOI: 10.3389/fnano.2023.1057422
[4] Degl'Innocenti R et al 2017 *J. Phys. D: Appl. Phys*. **50** 174001
[5] Degl'Innocenti R et 2016 *ACS Photon.* **3**(10) 1747−53.
[6] Yu X, Suzuki Y, Van Ta M, Suzuki S, Asada M 2021 *IEEE Electron Device Lett.* **42**(7) 982-5.
[7] Shen S, Liu X, Shen Y, Qu J, Pickwell-MacPherson E, Wei X, Sun Y 2022 *Adv. Optical Mater*. **10** 2101008.
[8] Hale L L. Keller J, Siday T, Hermans R I, Haase J, Reno, J L, Brener I, Scalari G, Faist J, Mitrofanov O 2020 *Laser Photonics Rev*. **202(**14) 1900254.
[9] Lu Y, Hale L L, Zaman A M, Addamane S J, Brener I, Mitrofanov O, Degl'Innocenti R 2023 *ACS Photon.* **10**(8), 2832–8.
[10] Hale L L, Siday T, Mitrofanov O 2023 *Opt. Mater. Express* **13**(11) 3068.
[11] Norman S, Seddon J, Lu Y, Hale L L, Zaman A M, Addamane S J, Brener I, Degl'Innocenti R, Mitrofanov O *submitted*.
[12] Degl'Innocenti R, Montinaro M, Xu J, Piazza V, Pingue P, Tredicucci A, Beltram F, Beere H E, Ritchie D A 2009 *Opt. Express* **17**, 23785-92
[13] Degl'Innocenti R et 2017 *ACS Photon.* **4**(9) 2150-7.
[14] Jansen C, Al-Naib I A I, Born N, Koch M 2011 *Appl. Phys. Lett.* **98**(5) 051109.
[15] Wu Y, Hu X, Ao Y, Zhao Y, Gong Q 2017 *Adv. Opt. Mater.* **5**(18) 1700357.
[16] Jeannin M et al 2019 *ACS Photon.* **6**(5) 1207-15.
[17] Joseph S, Pandey S, Sarkar S, Joseph J *Nanophoton*. 2021, 10(17), 4175-07.